Mechanical properties and phase stability of monoborides using density functional theory calculations

Hyojung Kim* and Dallas R. Trinkle†

Department of Materials Science and Engineering, University of Illinois at Urbana-Champaign, Urbana, Illinois 61801, USA

(Received 1 February 2017; revised manuscript received 9 May 2017; published 26 June 2017)

We compute the structural energies, elastic constants, and stacking fault energies, and investigate the phase stability of monoborides with different compositions $(X^1_{1-x}X^2_x)$B (X = Ti/Fe/Mo/Nb/V) using density functional theory in order to search for Ti monoborides with improved mechanical properties. Our computed Young's modulus and Pugh's modulus ratio, which correlate with stiffness and toughness, agree well with predictions from Vegard's law with the exceptions of mixed monoborides containing Mo and Fe. Among all the monoborides considered in this paper, TiB has the smallest Pugh's ratio, which suggests that the addition of solutes can improve the toughness of a Ti matrix. When X^1B and X^2B are respectively most stable in the B_{27} and B_f structures, the mixed monoborides $(X^1_{1-x}X^2_x)$B have a lower or similar stacking fault energy than TiB and could therefore improve the ductility of the Ti matrix. Among all $(X^1_{0.5}X^2_{0.5})$B, mixed $(Ti_{0.5}Mo_{0.5})$B and mixed $(Ti_{0.5}V_{0.5})$B have a higher Young's modulus, a higher Pugh's ratio, and a smaller stacking fault energy than TiB. We also construct phase diagrams and find large solubility limits for solid solutions containing Ti compared to those containing Fe.

DOI: 10.1103/PhysRevMaterials.1.013601

I. INTRODUCTION

Titanium alloys exhibit high hardness and corrosion resistance with low density, which makes them advantageous for aerospace and biomedical applications [1–3]. The strength and hardness of Ti alloys have been improved using grain refinement by precipitation formation [4]. Boron additions to Ti form TiB whiskers which improve the strength of Ti-matrix composites as the fraction of the TiB whiskers increases [4,5]. However, Ti alloys require further improvements to toughness for practical applications. Thus, solutes such as Fe, Mo, Nb, and V are added to stabilize the body-centered-cubic β-Ti phase [3,6,7], which has a higher toughness than the hexagonal-close-packed α-Ti phase. These solutes react to form ternary phases which could have higher stiffness and toughness compared to Ti monoborides. Monoborides with an improved toughness can directly be used as reinforcements within a Ti matrix [8] or as bulk ceramic phases [9]. However, it is difficult to measure the mechanical properties of Ti monoborides experimentally due to their needlelike microstructure [5], so we need a computational approach to optimize the properties of monoboride systems.

Many studies have investigated the mechanical properties of transition-metal monoborides XB (X = Ti/Fe/Mo/Nb/V) in their most stable crystal structure (FeB or CrB) [10–12], however, few studies [13,14] account for both crystal structures even though they are commonly observed in the form of stacking faults [7,15]. The FeB crystal structure has the Strukturbericht designation B_{27} (space group *Pnma*, No. 62), and the CrB crystal structure has the Strukturbericht designation B_f (space group *Cncm*, No. 63). These B_{27} and B_f structures are equiatomic phases with the same density [16]. Density functional theory (DFT) studies [11–13] computed the elastic constants of transition-metal monoborides and found that the strong interaction between boron atoms contributes significantly to the high stiffness. There are few DFT studies either on the structural properties or phase stabilities for ternary boride alloys such as (Ti,Nb)B [17] and transition-metal diboride [18] using a special quasirandom structure (SQS) method and showed reasonable agreement with experiments. Yeung *et al.* experimentally measured the structural and mechanical properties of (W,Ta)B monoborides with different compositions and found that $(W_{0.5}Ta_{0.5})$B has an enhanced hardness [19]. Many experimental studies focused on phase stabilities and suggested isothermal phase diagrams for transition-metal ternary boride systems such as Ti-V-B, Ti-Mo-B, and Ti-Nb-B [6,20,21]. However, we still need to understand the relations between the stiffness, toughness, ductility, and phase stability of ternary phases to design thermodynamically stable Ti monoborides with a high Young's modulus, high Pugh's ratio, and low stacking fault energies.

We present DFT calculations of the mechanical properties and phase stability of monoborides $(X^1_{1-x}X^2_x)$B (X = Ti/Fe/Mo/Nb/V). We study the various compositions of mixed monoborides using SQS for both B_{27} and B_f structures. The Young's modulus E measures the stiffness of a material which reflects the bonding strength within the material. We expect that the toughness (resistance to open a crack) and the ductility (ease of slip) of materials are correlated with Pugh's ratio [22] B/G and stacking fault energy (SFE) [23], respectively. Our computed E and B/G agree well with predictions from Vegard's law, with the exceptions of monoborides containing Mo and Fe. The computed stable SFEs of XB monoborides agree well with the axial next-nearest-neighbor Ising (ANNNI) model [24], and we assess the SFEs of mixed monoborides using this approximation. We also compute phase diagrams between different monoborides and find large solubility limits for Ti-containing monoborides compared to those containing Fe.

This paper is organized as follows: Section II describes the DFT computational details, Voigt-Reuss-Hill (VRH) approximations for polycrystalline elastic moduli, and the ANNNI model. Section III A compares the computed elastic moduli and Pugh's ratio of monoborides with the predictions from

*hkim378@illinois.edu
†dtrinkle@illinois.edu

Vegard's law and Sec. III B discusses the phase stability of mixed monoborides. Section III C investigates the stacking fault energies of monoborides for both B_{27} and B_f structures. Section IV provides further discussion and conclusions.

II. COMPUTATIONAL DETAILS

We perform density functional theory calculations using the Vienna *ab initio* simulation package (VASP) [25,26]. We use the projector-augmented wave (PAW) potentials generated by Kresse [27] with the Perdew-Wang91 (PW91) exchange-correlation functional [28]. The core electron configuration of the PAW potential we consider for each element is as follows: B = [He]$2s^2$, Ti = [Mg]$3p^6 3d^2 4s^2$, V = [Mg]$3p^6 3d^3 4s^2$, Fe = [Ar]$3d^6 4s^2$, Nb = [Zn]$4p^6 4d^4 5s^1$, and Mo = [Zn]$4p^6 4d^5 5s^1$. A plane-wave energy cutoff of 520 eV ensures an energy convergence of less than 1 meV/atom. A $12 \times 8 \times 8$ and a $8 \times 12 \times 8$ Monkhorst-Pack [29] k-point grid integrates the band structure over the Brillouin zone of the $1 \times 3 \times 2$ and $2 \times 1 \times 3$ supercells (48 atoms) of the B_{27} and B_f structures, respectively. We employ Methfessel-Paxton [30] smearing with an energy width of 0.15 eV. The force on each atom in the relaxed supercells is less than 5 meV/Å. We generate SQSs for mixed borides using the ATAT program [31] and all the calculations for Fe-containing systems are spin polarized. We compute the nine independent elastic stiffness coefficients for orthorhombic monoborides by applying strains with magnitudes ranging from -0.4% to 0.4% with a 0.1% interval, relaxing the atomic degrees of freedom while keeping the cell volume fixed and fitting the stress response to strain [17]. The elastic stiffness coefficient data of NbB and the mixed monoboride $(Ti_{0.5}Nb_{0.5})B$ in the B_{27} structure are taken from Trinkle [17], who employed similar DFT parameters as in our study.

We use the Voigt-Reuss-Hill (VRH) approximation [32–34] to estimate the polycrystalline elastic properties of mixed monoborides by averaging the computed anisotropic elastic moduli, and compare the results to those obtained from Vegard's law [35]. The upper bounds on the bulk modulus B and the shear modulus G are given by the Voigt approximation Eq. (1) [32], while the lower bounds on B and G are given by the Reuss approximation Eq. (2) [33],

$$\begin{aligned} B_{\mathrm{V}} &= \frac{1}{9}(C_{11}+C_{22}+C_{33}) + \frac{2}{9}(C_{12}+C_{23}+C_{13}), \\ G_{\mathrm{V}} &= \frac{1}{15}(C_{11}+C_{22}+C_{33}) - \frac{1}{15}(C_{12}+C_{23}+C_{13}) \\ &\quad + \frac{1}{5}(C_{44}+C_{55}+C_{66}), \end{aligned} \tag{1}$$

$$\begin{aligned} \frac{1}{B_{\mathrm{R}}} &= (S_{11}+S_{22}+S_{33}) + 2(S_{12}+S_{23}+S_{13}), \\ \frac{1}{G_{\mathrm{R}}} &= \frac{4}{15}(S_{11}+S_{22}+S_{33}) - \frac{4}{15}(S_{12}+S_{23}+S_{13}) \\ &\quad + \frac{1}{5}(S_{44}+S_{55}+S_{66}), \end{aligned} \tag{2}$$

where C and S are the elastic stiffness and compliance tensors, respectively. The VRH approximation for $B = (B_{\mathrm{V}} + B_{\mathrm{R}})/2$ and the VRH approximation for $G = (G_{\mathrm{V}} + G_{\mathrm{R}})/2$. Then, Pugh's modulus ratio is defined to B/G and Young's modulus E is

$$E = \frac{9BG}{3B+G}. \tag{3}$$

We compare these values to those obtained from Vegard's law [35], which approximates the property of the alloy with respect to the concentration of each constituent in a linear relation.

We directly compute the stacking fault energies of monoborides XB in the B_{27} and B_f structures by constructing supercells containing stacking faults. The stacking fault energy (SFE) is the total energy difference per area A between two supercells with (E_{s}) and without (E_{p}) a stacking fault

$$\mathrm{SFE}_{B_{27}} = \frac{E_{\mathrm{s}} - E_{\mathrm{p}}}{A_{B_{27}}}, \tag{4}$$

$$\mathrm{SFE}_{B_f} = \frac{E_{\mathrm{s}} - E_{\mathrm{p}}}{A_{B_f}}. \tag{5}$$

We apply alias shear [36] to construct a single stacking fault in the $2 \times 1 \times 1$, $3 \times 1 \times 1$, and $4 \times 1 \times 1$ supercells.

The ordering of common structural units in the B_{27} and B_f structures enables us to estimate the stable stacking fault energies of monoborides using the axial next-nearest-neighbor Ising (ANNNI) model [24]. The stacking disorders of structural units (***A*** and ***B***, discussed in Fig. 4) between B_{27} and B_f are similar to the atomic disorder between fcc and hcp in that changing the atomic arrangements in one structure creates another structure as an intrinsic or extrinsic stacking fault. Sandlöbes *et al.* found that the stacking fault energies in Mg alloys are well described using the energy difference between fcc and hcp structures by considering up to the second nearest interlayer interactions [23]. Here, we employ the ANNNI model for calculating the stacking fault energies of the B_{27} and B_f structures, which have commonly repeated structural units along the [100] direction as . . . ***ABABA*** . . ., and . . . ***BBB*** . . . (or . . . ***AAA*** . . .), respectively. Considering only the next-nearest-neighbor structural unit interactions, the stacking fault energy (SFE) of the system is the energy difference between the B_{27} and B_f unit cells per stacking fault area A,

$$\mathrm{SFE}_{B_{27}} = \frac{E(B_f) - E(B_{27})}{A_{B_{27}}}, \tag{6}$$

$$\mathrm{SFE}_{B_f} = \frac{E(B_{27}) - E(B_f)}{A_{B_f}}. \tag{7}$$

Using the ANNNI model rather than the direct DFT calculation to compute the stacking fault energy is advantageous since it avoids the expensive large supercell calculations required to minimize the interactions between stacking faults. In addition, the ANNNI model may be more realistic than a direct calculation for an SQS model where the stacking fault construction in the supercell does not guarantee a random local environment near the fault.

III. RESULTS AND DISCUSSION

A. Elastic moduli of monoborides

Figure 1 shows the two crystal structures of monoborides (B_{27} and B_f) considered in this study and that they are distorted versions of each other. Both B_{27} and B_f structures

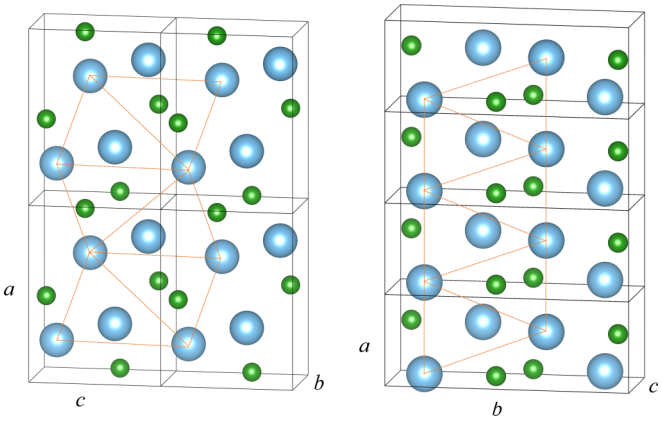

FIG. 1. The B_{27} (left) and B_f (right) structures of transition-metal monoborides XB, where X atoms (X = Ti/Fe/Mo/Nb/V) are represented by large blue spheres and B atoms are shown as small green spheres. The atoms connected by orange lines are in the same plane and are repeated with different orientations in the B_{27} and B_f structures, showing that they are distorted versions of each other (discussed in Fig. 4). The lattice parameters of the B_{27} and B_f structures closely match in different directions: $2a$, b, and $3c$ of B_f are similar to a, $3b$, and $2c$ of B_{27}. For example, TiB in the B_{27} structure has lattice parameters $a = 6.116$ Å, $b = 3.048$ Å, and $c = 4.560$ Å, while TiB in the B_f structure has lattice parameters $a = 3.287$ Å, $b = 8.487$ Å, and $c = 3.053$ Å.

have unit cells containing four transition-metal atoms X (X = Ti/Fe/Mo/Nb/V) in the $4c_1$ Wyckoff position and four B atoms in the $4c_2$ position. The fractional coordinates of the $4c_1$ and $4c_2$ positions are (0.177,0.25,0.123) and (0.029,0.25,0.603) in the B_{27} structure, and (0,0.146,0.25) and (0,0.44,0.25) in the B_f structure, respectively. Both structures consist of common structural units (discussed in Fig. 4), and they can be generated from each other by sliding one structure in a particular direction with reshuffling of the boron atoms [16]. The zigzag chain of boron atoms, known to contribute to the high stiffness of monoborides [11], points along the b direction of the B_{27} structure, which corresponds to the c direction of the B_f structure. We find that TiB and FeB are more stable in the B_{27} structure by energy differences of 10.5 and 6.8 meV/f.u. relative to B_f, respectively, where each formula unit contains two atoms. The MoB, VB, and NbB are more stable in the B_f structure by energy differences of 50.45, 16.9, and 10.3 meV/f.u. relative to B_{27}, respectively. These relative stabilities agree qualitatively with experiments [10,37,38].

Figure 2 shows the computed E and B/G values of monoborides, indicating that the values of mixed monoborides agree well with the results estimated by Vegard's law (e.g., the straight lines that would connect the values of constituent monoborides X^1B and X^2B). In most cases the E values of mixed monoborides $(X^1_{0.5}X^2_{0.5})$B are similar (within 10%) to the values predicted by Vegard's law, with the exceptions of mixed monoborides containing either Mo or Fe. In particular, $(Ti_{0.5}Mo_{0.5})$B and $(Fe_{0.5}Nb_{0.5})$B deviate the most positively and negatively from Vegard's law, which raises a question about the stability of these materials as a random solid solution as either B_{27} or B_f structure (discussed in Sec. III B). Based on our calculation using the SQS model, the mixed $(X^1_{0.5}X^2_{0.5})$B of (Ti,Mo)B, (Ti,V)B, (Nb,V)B, (Mo,Nb)B, (Mo,V)B, and (Ti,Nb)B systems have higher E (i.e., stiffness) than TiB. However, some of the mixed monoborides such as $(Ti_{0.5}Mo_{0.5})$B and $(Mo_{0.5}V_{0.5})$B are not predicted by Vegard's law as mixed monoborides with a higher Young's modulus than TiB, when considering the two constituent monoborides as the B_{27} structure. The shear modulus G (not shown here) has the same trend as E. Pugh's ratio estimates the toughness of the materials, where $B/G \gtrsim 1.75$ indicates tough materials while $B/G \lesssim 1.75$ indicates brittle materials [22]. Among all the monoborides shown here, TiB has the smallest B/G value, which leads to the possibility of improving the toughness of TiB with the presence of solutes in the Ti matrix. Although the computed B/G using SQS agrees well with the estimation from Vegard's law for most of the mixed monoborides, the B/G of mixed $(Fe_{0.5}Mo_{0.5})$B as both B_{27} and B_f structures does not follow well with the Vegard's law estimations. The tabular form of bulk modulus B, shear modulus G, and Young's

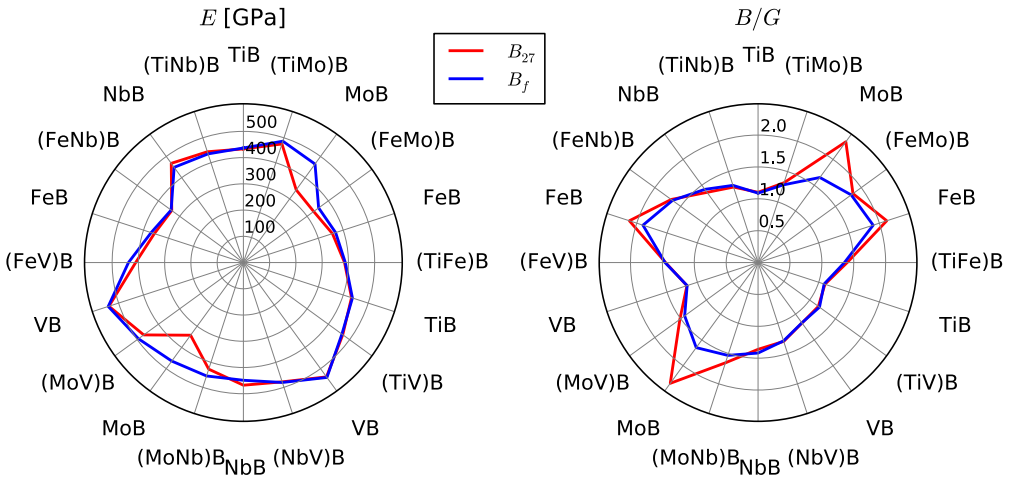

FIG. 2. Polycrystalline elastic properties of XB (X = Ti/Fe/Mo/Nb/V) and $(X^1_{0.5}X^2_{0.5})$B. The Young's modulus E in GPa (left) and Pugh's modulus ratio B/G (right) of each monoboride in both of B_{27} and B_f structures are shown. The E and B/G values are similar between both crystal structure types and agree well with the estimations from Vegard's law for most of the monoborides, except the ones containing Mo and Fe.

modulus E as well as the lattice parameters of XB, and mixed $(X^1_{0.5}X^2_{0.5})$B for both structures are available [39].

The deviations from Vegard's law in Young's modulus are also reflected in the volume (lattice parameter) of mixed borides. We find that the variation in volume is largest for the FeB-NbB system and smallest for the TiB-MoB system. This is because of the difference in volume of constituent monoborides (i.e., FeB < VB < MoB ⩽ TiB < NbB) which can be explained by the same trend of Seitz radii of the elements (i.e., Fe < V < Mo < Ti < Nb) [40]. We note that the volumes of $(Ti_{0.5}Mo_{0.5})$B and $(Fe_{0.5}Nb_{0.5})$B show the largest deviation from the Vegard's law estimations negatively (by -8 Å^3 for a 48-atom supercell) and positively (by 13 Å^3 for a 48-atom supercell), respectively. The deviation from Vegard's law for (Ti,Mo)B implies that the mixing affects the electronic structure around the Ti and Mo atoms and induces a different environment from Ti in TiB and Mo in MoB. Compared to Vegard's law predictions, the mixed $(Ti_{0.5}Mo_{0.5})$B has a smaller volume, indicating stronger interatomic bonding which leads to a larger Young's modulus. On the other hand, the mixed $(Fe_{0.5}Nb_{0.5})$B has a larger volume, indicating a weaker interatomic bonding which results in a lower Young's modulus. We investigated the applicability of Vegard's law for estimating Pugh's ratio and stacking fault energy, but they do not exhibit similar trends as Young's modulus and volume. We expect Pugh's ratio and stacking fault energy to correlate with more complex environmental factors beyond atomic bonding.

B. Phase stability of mixed monoborides

We compute the total energies of mixed monoborides $(X^1_{1-x}X^2_x)$B (X = Ti/Fe/Mo/Nb/V) in both B_{27} and B_f structures for $x = 0, \frac{1}{24}, \frac{1}{4}, \frac{1}{2}, \frac{3}{4}, \frac{23}{24}$, and 1. We fit these energies with cubic splines to construct binary phase diagrams of X^1B$-X^2$B systems to explain the relative stability in pseudobinary systems between the B_{27} and B_f structures. The Gibbs free energy G of an $(X^1_{1-x}X^2_x)$B as a function of composition x is

$$G = H - TS = H + k_{\mathrm{B}}T[x\ln x + (1-x)\ln(1-x)], \quad (8)$$

where H is the mixing enthalpy, T is the temperature in degrees Kelvin, S is the configurational entropy, and k_{B} is the Boltzmann constant. The common tangent points of fitted Gibbs free energy curves represent the equilibrium compositions (i.e., the solubility limit) of solutes in the X^1B and X^2B phases for each temperature.

We find a large solubility limit in mixed monoborides containing Ti compared to those containing Fe. The solubility limits of Nb, V, and Mo in TiB are above 0.30 at 1600 K, which are comparable to the reported experimental results: TiB dissolves the Nb, V, and Mo up to 0.4, 0.5, and 0.34, respectively, and the solubility limits of Ti in NbB, VB, and MoB are 0.3, 0.15, and 0.64, respectively, at around 1400 °C [6,20,21]. The ternary systems containing Fe, such as FeB-VB, FeB-MoB, and FeB-NbB, have a low solubility (less than 0.05) and are unlikely to exist as a random solid solution either as B_{27} or B_f structures over a majority of the monoboride composition range. This difference in solubility trend between monoborides containing Ti and Fe is possibly due to the large differences in the number of valence electrons between Fe (in group VIII) and solutes V, Nb, and Mo (in groups V and VI), compared to those differences between Ti (in group IV) and the solutes, based on the Hume-Rothery rules which suggest the same valence elements tend to have an extensive solid solubility [41]. We find that the mixed monoborides where two constituent monoborides are most stable as B_f structures (i.e., VB, MoB, and NbB) are stable as B_f structures across the full composition range for the entire temperature range. On the other hand, for the TiB-FeB system where both of the constituent monoborides are most stable as B_{27} structures, the solubilities are small and there are even mixed monoboride compositions that are stable as B_f structures. A possible reason is the large difference between ionic radii of Fe and Ti which may cause the crystal structures to distort easily from one to another, however, this requires further studies to validate the occurrence of B_f structure stable phases for the mixture of TiB and FeB.

Figure 3 shows the solubility limits in the FeB-NbB and TiB-MoB systems which show a significant deviation of E from Vegard's law predictions. The solubility of Fe in NbB and of Nb in FeB is low (<0.001) even at a high temperature (2000 K), showing that the mixed monoborides with compositions between these solubility limits are unlikely to exist as both B_{27} and B_f structures for the entire temperature

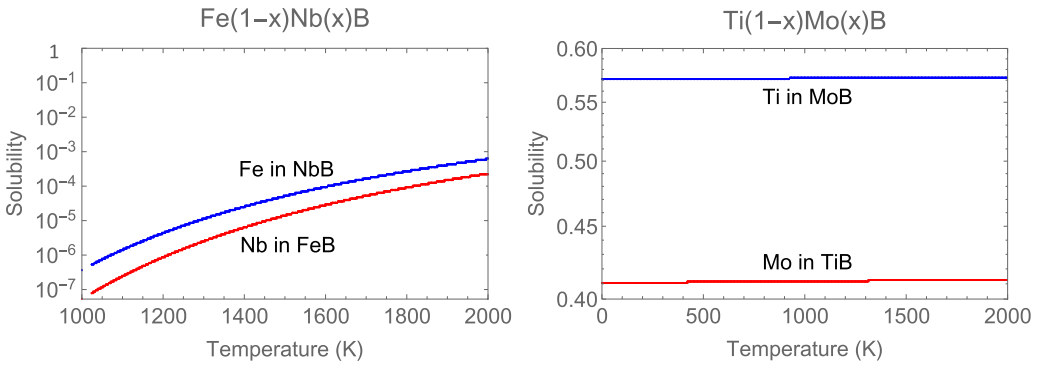

FIG. 3. Solubility limits in FeB-NbB system from 1000 to 2000 K, and in TiB-MoB system from 0 to 2000 K. The solubility of Nb in FeB (B_{27} structure) and of Fe in NbB (B_f structure) is very small, less than 0.001 even at 2000 K. In contrast, there is a large solubility in TiB-MoB system: The solubility limit of Mo in TiB (B_{27} structure) is 0.411–0.413 and of Ti in MoB (B_f structure) is 0.570–0.573 over the entire temperature range from 0 to 2000 K.

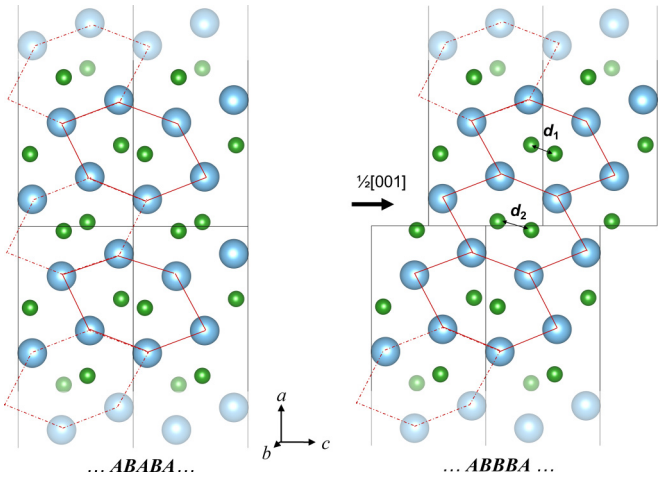

FIG. 4. B_{27} structure (left) and stacking fault formation (right) on the (200) plane in the $\frac{1}{2}[001]$ direction. The B_{27} structure consists of structural units $\boldsymbol{A}$ and $\boldsymbol{B}$, where $\boldsymbol{A}$ has six metal atoms connected with dashed lines, including the two boron atoms inside it, while $\boldsymbol{B}$ has six metal atoms connected with solid lines and two boron atoms inside it. The B_f structure consists of only one type of structural unit $\ldots \boldsymbol{BBB} \ldots$ (or $\ldots \boldsymbol{AAA} \ldots$) and is generated by creating an intrinsic or extrinsic stacking fault in the B_{27} structure, and vice versa. Additionally, it requires the reshuffling of boron atoms at the stacking fault to form the same $\boldsymbol{B}$ unit far from the stacking fault so that the distance d_2 between boron atoms at the stacking fault becomes close to the ideal distance between boron atoms d_1 away from the fault.

range. Thus we expect that most of the FeB-NbB monoboride compositions, including $(Fe_{0.5}Nb_{0.5})B$, will exist as an ordered mixture of the ternary system. Also, we attribute the significant small value of E for mixed $(Fe_{0.5}Nb_{0.5})B$ compared to the estimations of Vegard's law to the unfavorable phases of this composition as a random solid solution. On the other hand, the solubility of Ti in MoB and of Mo in TiB is large (0.57 and 0.41, respectively) and varies little with temperature, showing that most of the mixed monoborides (Ti,Mo)B, including $(Ti_{0.5}Mo_{0.5})B$, are stable as either B_{27} or B_f structures. Based on the significantly larger E of $(Ti_{0.5}Mo_{0.5})B$ compared to the Vegard's law prediction and its stability as a mixed phase, we expect that $(Ti_{0.5}Mo_{0.5})B$ and a possibly wide range of compositions in the TiB-MoB system are promising candidates for Ti-matrix composites with improved stiffness and toughness.

C. Stacking fault energy

Figure 4 shows that the stacking fault in the B_{27} structure has the same local environment as the B_f structure and vice versa. The orientational relationship between the two crystal structures has been observed experimentally using high-resolution transmission electron microscopy: $(100)\,B_{27} \| (110)\,B_f$ and $[010]\,B_{27} \| [001]\,B_f$ in Ti-B alloys [7,15,42,43]. The TiB grows as the B_{27} structure, which is the most stable state, and generates stacking faults in the form of the B_f structure (metastable state) during growth. The B_{27} structure unit cell consists of $\boldsymbol{AB}$ structural units and the B_f structure unit cell consists of $\boldsymbol{AA}$ (or $\boldsymbol{BB}$) structural units, where $\boldsymbol{A}$ and $\boldsymbol{B}$ are defined in Fig. 4. The $\boldsymbol{A}$ and $\boldsymbol{B}$ units can be generated from each other by a shift along the $\frac{1}{2}[001]$ direction on the (200) plane of the B_{27} structure or a shift along the $\frac{1}{4}[1\bar{1}0]$ direction on the (110) plane of the B_f structure, and unfault by reverse displacements. However, this does not occur only by a simple shear, but also requires boron reshuffling near the fault plane. For example, in TiB we find that the distance between boron atoms at the fault plane (d_2) decreases from 2.064 to 1.816 Å after relaxation, becoming much closer to the ideal distance between boron atoms (d_1) of 1.828 Å. The boron reshuffling lowers the energy of the system while creating well matching $\boldsymbol{B}$ structural units at the stacking fault region in Fig. 4.

TABLE I. Stable stacking fault energies (SFEs) of monoborides. The stacking faults are in the $\frac{1}{2}[001]$ direction on the (200) plane of the B_{27} structure and in the $\frac{1}{4}[1\bar{1}0]$ direction on the (110) plane of the B_f structure. We compute SFEs directly using Eqs. (4) and (5), and the values listed in the table are extrapolated for an infinite number of atoms N based on the calculations where $N = 16$, 24, and 32 for the B_{27} structure and $N = 16$ and 32 for the B_f structure. The SFEs are also estimated by the ANNNI model using Eqs. (6) and (7). The ANNNI model provides good estimates of the stable SFEs of monoborides with a maximum deviation of about 26 mJ/m^2 for NbB.

SFE (mJ/m^2)	TiB	FeB	MoB	VB	NbB
Direct calculation (in B_{27})	48.4	28.0	−233.5	−69.7	−17.3
ANNNI model (in B_{27})	48.0	36.7	−230.0	−84.0	−43.8
Direct calculation (in B_f)	−48.5	−41.2	244.1	84.5	56.6
ANNNI model (in B_f)	−48.2	−36.5	228.7	84.5	44.1

Table I shows agreement between the stable stacking fault energy computed directly from DFT and the ANNNI model for both B_{27} and B_f structures. We compute the stacking fault area of the (200) plane in the B_{27} structure and of the (110) plane in the B_f structure for each monoboride using the lattice parameters from the relaxed geometries. The positive stacking fault energies for TiB and FeB in the B_{27} structure indicate that they are more stable as B_{27} than as the B_f structure, which is consistent with the total energy comparison shown in Sec. III A. The small differences between the direct calculation and ANNNI model suggest that accounting for interactions between adjacent structural units only yields a good approximation for computing stacking fault energies, and also avoids computationally expensive calculations requiring large supercells for the stacking fault energy of mixed monoborides. The maximum deviation between the two approaches occurs for NbB, which may requires higher-order interaction parameters in the ANNNI model to improve the agreement with the direct calculations.

Figure 5 shows the estimated stable stacking fault energies (SFEs) of monoborides computed using the ANNNI model, suggesting that mixed monoborides have lower SFEs than TiB. The mixed monoborides containing Ti or Fe except for $(Fe_{0.5}V_{0.5})B$ tend to have low SFEs. In particular, the mixed $(X^1_{0.5}X^2_{0.5})B$ of (Ti,Mo)B, (Ti,V)B, (Ti,Fe)B, and (Fe,Nb)B systems have lower SFEs than TiB, indicating that the mixed monoborides could have improved ductility. Among those, mixed $(Ti_{0.5}Mo_{0.5})B$ and $(Ti_{0.5}V_{0.5})B$, which have higher E, B/G, and lower SFEs than TiB, are promising candidates for aerospace and biomedical applications. We note that Vegard's

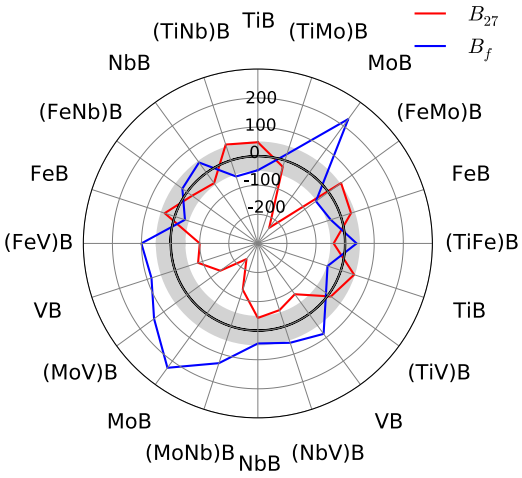

FIG. 5. The stable stacking fault energy SFE (mJ/m^2) of mixed $(X^1_{0.5}X^2_{0.5})$B computed using the ANNNI model for both the B_{27} and B_f structures. The SFEs for the B_{27} and B_f structures are calculated using Eqs. (6) and (7), respectively. A negative SFE indicates instability in that crystal structure and the monoboride is more likely to stay in the other crystal structure. The monoborides with the SFEs close zero are expected to slip more easily under shear. The shaded area corresponds to the SFE of TiB, ± 48 mJ/m^2.

law approximates the larger magnitude of SFE of mixed $(Ti_{0.5}Mo_{0.5})$B than that of TiB when considering the two constituent monoborides as the B_{27} structure, which draws different conclusions between Vegard's law and the SQS model as to whether mixed $(Ti_{0.5}Mo_{0.5})$B would improve the ductility of Ti monoborides. Although mixed $(Fe_{0.5}Nb_{0.5})$B and $(Ti_{0.5}Fe_{0.5})$B have a lower SFE than TiB, they have a lower Young's modulus than TiB (see Sec. III A) and low solubilities (see Sec. III B) which makes them practically undesirable as mixed monoborides for a wide composition range. Also, despite the Pugh's ratio of MoB as the B_{27} structure has the highest value (see Fig. 2), implying the highest toughness among all the monoborides considered in this study, it is unlikely to exist as a bulk or even in the form of a stacking fault as the B_f structure. Similarly, the mixed monoborides $(X^1_{0.5}X^2_{0.5})$B of (Mo,Nb)B, (Mo,V)B, and (V,Nb)B systems are stable in the B_f structure and require higher energy than TiB to create a stacking fault, i.e., a portion of the B_{27} structure, from their stable structure. The tabular forms of the stacking fault energies of XB, and mixed $(X^1_{0.5}X^2_{0.5})$B for both structures are available [39].

IV. CONCLUSION

We studied the polycrystalline mechanical properties and phase stabilities of transition-metal monoborides XB and $(X^1_{1-x}X^2_x)$B (X = Ti/Fe/Mo/Nb/V) in both of the FeB (B_{27}) and CrB (B_f) crystal structures using density functional theory calculations. We find that the computed Young's modulus, Pugh's modulus ratio, and stacking fault energy of $(X^1_{0.5}X^2_{0.5})$B using a special quasirandom structure deviate from the predictions of Vegard's law in cases containing Fe or Mo. These deviations lead to different conclusions whether the mixed monoborides may have a higher Young's modulus, and a lower stacking fault energy than TiB. The mixed monoborides containing Fe have low solubilities and are less likely to exist as a random solid solution either in the B_{27} or B_f structure for most of the composition range. We find that both the MoB-VB and MoB-NbB systems are stable as the B_f structure for the entire composition range, and these mixed monoborides require a high energy to create a stacking fault compared to TiB, which is not desirable for improving ductility.

This work searches for potential Ti monoborides with a high Young's modulus, high Pugh's ratio, and low stacking fault energy for applications in the aerospace and biomedical fields. We find that TiB has the smallest Pugh's ratio among monoborides and therefore expect that the presence of solutes could improve the toughness of the Ti matrix. The mixed monoborides containing Ti have a large solubility and show a lower or similar stacking fault energy than TiB, indicating a higher ductility than TiB. In particular, mixed $(Ti_{0.5}Mo_{0.5})$B and $(Ti_{0.5}V_{0.5})$B are promising for their higher E, B/G, and lower stacking fault energy than TiB, along with their phase stability over a large composition and temperature range.

This computational approach is not limited to specific solutes or monoboride systems, and can be applied to monoborides and diborides with other solutes or other quaternary (or even higher-order) ceramic phases and provides a guide to tailor their structural properties and phase stabilities. Also, from the crystal orientation relationship between the B_{27} and B_f structures, we find that the direct calculation of the stable stacking fault energy of monoborides agrees well with the axial next-nearest-neighbor Ising (ANNNI) model, which is applicable to more complex ceramic phases and saves computational time. We expect these results will help suggest optimal metallic borides for Ti-based alloys and bulk ceramics and can be verified by complementary experiments.

ACKNOWLEDGMENTS

Figures 1 and 4 are drawn using the VESTA program [44]. This research was supported by NSF/DMREF Grant No. 1435545. This work used the Extreme Science and Engineering Discovery Environment (XSEDE), which is supported by National Science Foundation grant number ACI-1053575 [45].

The full data set, including input and output files, is available through the Materials Data Facility; see Ref. [39].

[1] R. R. Boyer and R. D. Briggs, J. Mater. Eng. Perform. **14**, 681 (2005).
[2] H. Rack and J. Qazi, Mater. Sci. Eng. C **26**, 1269 (2006).
[3] E. Eisenbarth, D. Velten, M. Müller, R. Thull, and J. Breme, Biomaterials **25**, 5705 (2004).
[4] J. Zhu, A. Kamiya, T. Yamada, W. Shi, and K. Naganuma, Mater. Sci. Eng. A **339**, 53 (2003).
[5] K. B. Panda and K. S. Ravi Chandran, Metall. Mater. Trans. A **34**, 1993 (2003).
[6] L. Artyukh, D. Borysov, A. Bondar, P. Martsenyuk, N. Tsyganenko, and T. Velikanova, High. Temp. Mater. Process. **25**, 75 (2006).
[7] U. Kitkamthorn, L. Zhang, and M. Aindow, Intermetallics **14**, 759 (2006).

[8] T. Velikanova, A. Bodar, L. Artyukh, O. Bilous, S. Firstov, and D. Miracle, Titanium-boride composites, in *Metallic Materials with High Structural Efficiency*, edited by O. N. Senkov, D. B. Miracle, and S. A. Firstov (Springer, Dordrecht, 2004), pp. 259–268.
[9] K. Takagi, J. Solid State Chem. **179**, 2809 (2006).
[10] P. Mohn and D. G. Pettifor, J. Phys. C: Solid State Phys. **21**, 2829 (1988).
[11] K. Panda and K. R. Chandran, Acta Mater. **54**, 1641 (2006).
[12] A. Gueddouh, B. Bentria, and I. K. Lefkaier, J. Magn. Magn. Mater. **406**, 192 (2016).
[13] X. Xu, K. Fu, L. Li, Z. Lu, X. Zhang, Y. Fan, J. Lin, G. Liu, H. Luo, and C. Tang, Physica B **419**, 105 (2013).
[14] B. Huang, Y.-H. Duan, W.-C. Hu, Y. Sun, and S. Chen, Ceram. Int. **41**, 6831 (2015).
[15] H. Feng, Y. Zhou, D. Jia, and Q. Meng, Scr. Mater. **55**, 667 (2006).
[16] D. Hohnke and E. Parthé, Acta Crystallogr. **20**, 572 (1966).
[17] D. Trinkle, Scr. Mater. **56**, 273 (2007).
[18] B. Alling, H. Högberg, R. Armiento, J. Rosen, and L. Hultman, Sci. Rep. **5**, 9888 (2015).
[19] M. T. Yeung, R. J. Lei, C. L. Turner, Y. Wang, S. H. Tolbert, and R. B. Kaner, Adv. Mater. **28**, 6993 (2016).
[20] O. A. Potazhevska, A. A. Bondar, L. A. Duma, V. M. Petyukh, V. B. Sobolev, and T. Y. Velikanova, Powder Metall. Met. Ceram. **53**, 230 (2014).
[21] D. B. Borisov, L. V. Artyukh, A. A. Bondar, P. S. Martsenyuk, A. V. Samelyuk, N. I. Tsiganenko, O. S. Fomichov, and T. Y. Velikanova, Powder Metall. Met. Ceram. **46**, 58 (2007).
[22] S. F. Pugh, Philos. Mag. Ser. 7 **45**, 823 (1954).
[23] S. Sandlöbes, M. Friàk, S. Zaefferer, A. Dick, S. Yi, D. Letzig, Z. Pei, L.-F. Zhu, J. Neugebauer, and D. Raabe, Acta Mater. **60**, 3011 (2012).
[24] W. Selke, Phys. Rep. **170**, 213 (1988).
[25] G. Kresse and J. Hafner, Phys. Rev. B **47**, 558 (1993).
[26] G. Kresse and J. Furthmüller, Comput. Mater. Sci. **6**, 15 (1996).
[27] G. Kresse and D. Joubert, Phys. Rev. B **59**, 1758 (1999).
[28] J. P. Perdew, in *Electronic Structure of Solids '91*, edited by P. Ziesche and H. Eschrig (Akademie Verlag, Berlin, 1991), pp. 11–20.
[29] H. J. Monkhorst and J. D. Pack, Phys. Rev. B **13**, 5188 (1976).
[30] M. Methfessel and A. T. Paxton, Phys. Rev. B **40**, 3616 (1989).
[31] A. Van de Walle, M. Asta, and G. Ceder, CALPHAD **26**, 539 (2002).
[32] W. Voigt, *Lehrbuch der Kristallphysik* (Teubner, Leipzig, 1928), p. 962.
[33] A. Reuss, Z. Angew. Math. Mech. **9**, 49 (1929).
[34] R. Hill, Proc. Phys. Soc., London, Sect. A **65**, 349 (1952).
[35] A. R. Denton and N. W. Ashcroft, Phys. Rev. A **43**, 3161 (1991).
[36] M. Jahnàtek, J. Hafner, and M. Krajčí, Phys. Rev. B **79**, 224103 (2009).
[37] B. F. Decker and J. S. Kasper, Acta Crystallogr. **7**, 77 (1954).
[38] O. Schob and E. Parthé, Acta Crystallogr. **19**, 214 (1965).
[39] H. Kim and D. R. Trinkle, Data citation: Mechanical properties and phase stability of monoborides using density functional theory calculations, http://dx.doi.org/doi:10.18126/M24S3J (2017).
[40] H. W. King, J. Mater. Sci. **1**, 79 (1966).
[41] W. F. Smith and J. Hashemi, *Foundations of Materials Science and Engineering*, 5th ed. (McGraw-Hill, New York, 2010), pp. 150–153.
[42] M. D. Graef, J. Löfvander, C. McCullough, and C. Levi, Acta Metall. Mater. **40**, 3395 (1992).
[43] B. Kooi, Y. Pei, and J. D. Hosson, Acta Mater. **51**, 831 (2003).
[44] K. Momma and F. Izumi, J. Appl. Crystallogr. **41**, 653 (2008).
[45] J. Towns, T. Cockerill, M. Dahan, I. Foster, K. Gaither, A. Grimshaw, V. Hazlewood, S. Lathrop, D. Lifka, G. Peterson, R. Roskies, J. Scott, and N. Wilkins-Diehr, Comput. Sci. Eng. **16**, 62 (2014).